JOURNAL OF APPLIED ELECTROCHEMISTRY **28** (1998) 80–88

Thermal effects of a laser beam on the electrodeposition of Ni–P alloys

I. ZOUARI*,‡, A. BELLAGI§, F. LAPICQUE*

* *Laboratoire des Sciences du Génie Chimique, CNRS–ENSIC–INPL, PO Box 451, F-54001 Nancy, France*
‡ *Ecole Nationale d'Ingénieurs de Gabès, Route de Medenine, 6029 Gabès, Tunisia*
§ *Ecole Nationale d'Ingénieurs de Monastir, Route de Kairouan, 5000 Monastir, Tunisia*

Received 15 November 1996; revised 11 June 1997

The paper deals with the effects of an incident laser beam on electrodeposition of Ni–P alloys from dilute acetate solutions. The kinetics of separate reductions of Ni^{2+} and $H_2PO_2^-$ species were first investigated by linear sweep voltammetry, varying the hypophosphite concentration and the solution temperature: comparison of the kinetically limited current densities of the two reductions suggested that increasing temperature might reduce the significance of P codeposition. This tendency was confirmed by deposition runs carried out at controlled current. Deposition performance was discussed in terms of faradaic yield and deposit properties, namely P content together with the aspect and the structure of the alloys. Use of a continuous or pulsed laser beam was shown to reduce the P content in the deposit at high current densities; in some cases, amorphous structures were replaced by more crystalline forms with assistance of a laser beam.

Keywords: *Ni–P alloys*, *electrodeposition*, *acetate electrolyte*, *hypophosphite*, *continuous and pulsed laser*, *thermal effects*

List of symbols

C_b	bulk concentration ($mol\,m^{-3}$ or $mol\,dm^{-3}$)
C_s	surface concentration ($mol\,m^{-3}$ or $mol\,dm^{-3}$)
D	diffusion coefficient ($m^2\,s^{-1}$)
D_0	diffusion coefficient at infinite dilution ($m^2\,s^{-1}$)
E	electrode potential (V)
E_0°	standard potential (V)
F	Faraday constant, $96\,487\,C\,mol^{-1}$
i	current density ($A\,m^{-2}$)
i_k	kinetically limited current density ($A\,m^{-2}$)
i_L	limiting current density ($A\,m^{-2}$)
$i_{standard}$	kinetically limited current density at standard potential ($A\,m^{-2}$)
m	weight of metal or alloy deposited (kg)
M	molecular weight ($kg\,mol^{-1}$)
Q	electrical charge passed (A s)
R	gas constant, $8.314\,J\,K^{-1}\,mol^{-1}$
T	temperature (K)
x_P	weight content of phosphorous in the alloy

Greek letters

α	charge transfer coefficient
Φ_e	faradaic yield
μ	dynamic viscosity (Pa s)
ν	kinematic viscosity ($m^2\,s^{-1}$)
ν_e	number of electrons involved in the reaction
ω	rotation rate ($rad\,s^{-1}$)

1. Introduction

Ni–P alloys can be produced by various methods, such as chemical reduction of nickel in the presence of hypophosphite, electrodeposition, or high temperature processes in the liquid or vapour state. For this case, rapid quenching is known to favour amorphization of the alloys produced. It is usually admitted that the structure of Ni–P alloys is mainly influenced by the phosphorous content and that amorphous structure is obtained for a phosphorous content over 10–12 wt %. However, the transition between crystalline and amorphous structures cannot be defined so clearly: for instance, the existence of microcrystallites in the amorphous bulk was shown for P contents up to 13 wt % [1]. Heat treatment of amorphous alloys was also reported to result in formation of small crystallites Ni_xP_y with various stoichiometries and containing Ni [2, 3].

Whatever the source of phosphorous in the electrolyte solution–phosphorous acid, H_3PO_3, or hypophosphorous acid, H_3PO_2, the phosphorous to nickel ratio is higher in the deposits than in the electrolytes, for low to moderate concentrations of P compounds in the solution [1, 4–8]. In particular, P content near 10 wt % was attained using a 0.125 M nickel chloride, 0.015 M H_3PO_2 electrolytic bath [7]. This codeposition is often considered as a coinduced process because of the favoured deposition of phosphorous. In addition, the relative importance of phosphorous deposition

0021-891X

compared with the metal production rate is affected by the applied current density and the temperature.

The assistance of a laser beam in electrodeposition processes also allows significant increase in temperature of both the electrode surface and the electrolyte solution close to the irradiated surface [9]. Pulsed laser sources induce periodic sharp increase in temperature and, in zinc deposition, these sources were shown to result in higher current densities, reduction in grain size and coalescence phenomena attributed to zinc diffusion into the substrate [10]. Circulation of the solution hinders the laser effect due to the periodic quenching of the deposition surface and, considering the high temperature processes for the production of amorphous alloys, it is questionable whether quenching phenomena could favour or hinder the formation of amorphous alloys.

The structure of Ni–P alloy may therefore be expected to be affected by the assistance of a pulsed laser beam through the local enhancement of temperature and its sharp transient variation. The aim of this work was to investigate the thermal effect of a laser beam on Ni–P deposition in the variation of operating conditions, namely current density, assistance of pulsed or continuous laser beams and concentration of hypophosphorous acid. In particular, the concentration values were chosen to allow the growth of either crystalline or mostly amorphous alloys. The results were discussed in terms of faradaic yield of deposition and the deposit properties such as P content, aspect and structure.

2. Experimental details

2.1. *Electrolytic solutions*

Electrodeposition of Ni–P was carried out from acetate/acetic acid buffer solution to reduce the changes in pH near the electrode. 0.5 M acetic acid with 0.10 M sodium acetate acted as supporting electrolyte. 0.05 M nickel acetate was added to the solution and the concentration of sodium hypophosphite, NaH_2PO_2, was varied from 0.005 to 0.20 M. All products were of analytical grade (Prolabo, France).

The kinematic viscosity of the solutions was measured using a Ubbelhode tube and the electrical conductivities were determined using a XE120 conductimetric probe connected to a CDRV 62 conductimeter (Tacussel). Temperature was varied from 25 to 56 °C. Table 1 displays the values obtained for these two physical properties at 25 and 50 °C, together with the solution pH at 25 °C.

2.2. *Electrochemical investigations*

Voltammetric measurements were carried out at low scan rate at a rotating copper disc. The 99.9% copper substrate was polished with an abrasive paper made of 10 μm iron oxide particles and the average asperity was far below one micrometre. Potentials were measured with respect to a saturated Hg/Hg_2SO_4 electrode (+0.658 V vs NHE at 25 °C) and a platinum cylindrical sheet acted as a counter electrode. The electrodes were inserted in a laboratory glass cell provided with a water jacket for temperature control. Oxygen was removed by a continuous nitrogen flow maintained over the liquid during the measurements. Rotation rate was varied from 200 to 2000 rpm and the voltammetric curves were recorded for most cases at 5 mV s^{-1} from the rest potential, near −0.40 V vs NHE, to −1.25 V vs NHE. Voltammetric curves were corrected for ohmic drop by estimating the term for total primary distribution near the RDE taking into account the conductivity of the solution [11].

Deposition of Ni–P alloys was performed under forced convection in two different cells. For both cells, the laser beam, when used, lay perpendicular to the electrode plane and entered the cell through a quartz window. A few experiments were done with a continuous laser beam in a rectangular vessel open to air and the liquid was stirred by mechanical agitation. The other deposition runs were carried out in a parallel cell with a cross section of 20 mm × 80 mm, as described previously [10]. The counter electrode was a 20 mm × 80 mm platinized titanium sheet and a mercury sulfate reference electrode was located in such a way as to prevent flow disturbance.

The working electrode was a square 99.9% copper sheet of 1 mm thick × 20 mm length. The surface was insulated using scotch tape except in its active part which was a 10 mm × 10 mm zone for runs without laser beam, and a 4 mm diameter disc with an incident laser beam of pulsed or continuous nature.

The continuous laser was an ionized Argon source with a power of 52 mW at 350 nm on a 2 mm circular spot. The pulsed laser source was a YAG laser at 532 nm. The power averaged over one cycle was kept below 2 W and the optical setup allowed alignment of the laser beam and the active part of the electrode. The repetition rate was fixed at 30 Hz and the energy

Table 1. Physico-chemical properties of the solution used (0.05 M nickel acetate, 0.10 M sodium acetate and 0.5 M acetic acid), depending on the sodium hypophosphite concentration

Properties	*Temperature*/°C	$H_2PO_2^-$/mol dm^{-3}			
		0	*0.005*	*0.01*	*0.20*
pH	25	4.11	4.07	4.12	4.20
10^6 Viscosity /$m^2 s^{-1}$	25, 50	1.016, 0.644	0.969, 0.626	0.975, 0.620	1.050, 0.612
Electrical conductivity /$\Omega^{-1} m^{-1}$	25, 50	0.945, 1.356	1.085, 1.600	1.074, 1.593	2.078, 3.080

was delivered within 8×10^{-9} s. For both lasers used, the energy was not evenly distributed on the spot area and higher fluxes were allowed in the centre, as for Gauss' function.

2.3. *Deposit analysis*

The amount of alloy produced was estimated by weighing the copper electrode before and after deposition using an analytical balance (Sartorius): measurements done within 0.2 mg allowed fair precision for deposits with thickness over a few micrometres.

Chemical analysis of the solid obtained was carried out by electron probe microanalysis (Cameca SX 50). The voltage was fixed at 15 kV for a current in the wire near 70 nA. Calibration was made with samples of copper, nickel and Fe_2P. The thickness of the deposits allowed the signals of the copper substrate to be two orders of magnitude below those of Ni and P; the weight fraction of Ni and P were, however, corrected from the low signal of the substrate. X-ray diffraction measurements were performed in a θ–2θ goniometer with the alloys still attached to the copper substrate. The CuK_α radiation was generated at 35 kV and 20 mA.

The alloy deposited was removed mechanically from the substrate and dissolved in a small amount of 15 wt% nitric acid solution. The nickel concentration was determined by atomic absorption spectrophotometry after sufficient dilution of the nitric solutions obtained: this measurement gave a second estimate for the deposit weight, taking into account the amount of phosphorous in the solid.

3. Deposition electrochemistry

The electrochemical behaviour of the ground electrolyte solution was first investigated, allowing the experimental procedure for reproducible (i/E) curves to be defined. Satisfactory reproducibility was obtained without pre-treatment of the copper surface; in addition the presence of a 2 μm thick nickel layer did not affect the electrolytic response in a significant manner. The rotation rate was of minor effect on the curves. The residual current was expressed with the potential by Tafel-type laws in the range −0.45, −1.0 V vs NHE with temperature-dependent parameters.

The electrochemical reduction of nickel and hypophosphite ions in acetic buffer solutions was investigated separately prior to their simultaneous reduction.

3.1. *Nickel electrodeposition*

Significant hysteresis of the deposition current was observed for the first cycle. Subsequent cycles performed onto the partially Ni-covered electrode exhibited weaker hysteresis and were quite reproducible. The nickel deposition current was estimated from the corrected i/E curves by subtracting

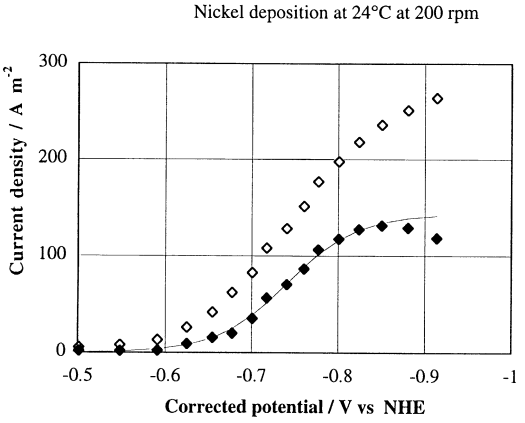

Fig. 1. Voltammetric curves of nickel deposition from a 0.05 M Ni acetate solution. Supporting electrolyte: 0.5 M acetic acid and 0.10 M sodium acetate. Overall current (light symbol) and reduction current (dark symbol) after subtracting the residual current; solid line corresponds to the deposition current fitted with the parameter values given in Table 2.

the residual current measured at the same temperature. The curves exhibited fair plateaus near −0.8 V vs NHE (Fig. 1). Nickel deposition has often been considered as a series of two electron transfers [12, 13] and the kinetics has been expressed by two Tafel laws in different potential ranges [13]. In the present case, an overall process was, however, assumed to represent the two-electron transfer involved in the metal formation. Voltammetric curves were interpreted using a classical model for the electrode reaction with diffusion phenomena at the rotating surface:

$$\frac{1}{i} = \frac{1}{i_k} + \frac{1}{0.621 v_e F C D^{2/3} \nu^{-1/6} \omega^{1/2}} \qquad (1)$$

where D is the diffusion coefficient of the electroactive species of bulk concentration C and ω is the rotation rate. Kinetically controlled current density i_k was expressed with reference to the standard potential E_0° of the Ni/Ni^{2+} couple (−0.250 V vs NHE at 25 °C)

$$i_k = i_{standard} \exp\left[-\frac{\alpha v_e F}{RT}\left(E - E_0^\circ\right)\right] \qquad (2)$$

$i_{standard}$ is the current density at E_0°. Fitting of the curves yielded estimates for the diffusion coefficient D and kinetic parameters $i_{standard}$ and αv_e. Figure 1 shows the experimental variations of the overall current and the partial current for nickel deposition; the simple model used holds for current densities over a few A m^{-2}, that is, for overpotentials more negative than −150 mV. Values of kinetic parameters and diffusion coefficient is shown in Table 2.

Diffusion of divalent nickel can be compared with its theoretical value at infinite dilution, D_0, which was calculated at 25 °C from the equivalent conductivity $\lambda_{Ni^{2+}}$ using the Nernst–Einstein relationship ($\lambda_{Ni^{2+}} = 50 \times 10^{-4}$ m^2 S mol^{-1} at 25 °C). Extrapolation to other temperatures was done using the Stokes–Einstein equation:

$$\frac{D\mu}{T} = \text{constant} \qquad (3)$$

Table 2. Diffusion coefficient of Ni^{2+} species and kinetics parameters of nickel deposition from a 0.05 M nickel acetate, 0.10 M sodium acetate, and 0.5 M acetic acid electrolytic bath

Temperature /°C	$i_{standard}$ /A m^{-2}	αv_e	$10^{10} \times D$ /m^2 s^{-1}	$10^{10} \times D_0$ /m^2 s^{-1}
24	8.0×10^{-4}	0.63	3.65	6.48
39	1.5×10^{-3}	0.73	8.49	9.23
56	3.9×10^{-3}	0.83	9.60	13.2

As expected, D was observed to be an increasing function of temperature and was significantly below its corresponding value at infinite dilution. The two kinetic parameters, αv_e and $i_{standard}$, also increased with temperature as shown in Table 2. The values of the overall charge transfer coefficient were slightly above published data, usually ranging from 0.43 [14, 15] to 0.5 according to Arvia *et al.* [16], and Saraby–Reintjes and Fleischmann [17]. However, the discharge of $NiOH^+$ species, being of significant concentration for pH over 4, was shown to occur with a charge transfer coefficient near 0.66 [18].

3.2. *Hypophosphite reduction*

The reduction of hypophosphite ion has been scarcely investigated and is often described by the following stoichiometry:

$$H_2PO_2^- + 2H^+ + e^- \rightarrow P + 2\,H_2O$$
$$E_0^\circ = -0.248\,V \text{ vs NHE}$$

Pure phosphorous cannot be produced electrolytically from aqueous media and it was suggested that formation of elemental phosphorous might occur during deposition of Ni–P alloys because the cathodic polarization of electrode required for Ni deposition assists in the deposition of phosphorous [4, 20]. The mechanism of phosphorous deposition is not well known [8] and an indirect pathway involving the intermediate formation of phosphine reducing Ni^{2+} species to form the alloy has been put into evidence in acidic media [19–21]. However the rate of phosphine evolution is of appreciable significance only for pH below 2 [20].

The presence of hypophosphite ion in the acetate buffer solution resulted in significant currents in the same potential range as for nickel deposition (Fig. 2); the current recorded in the range from −0.8 to −1 V vs NHE was observed to increase with the rotation rate, corresponding to a diffusion-controlled process. The current measured was assumed to be attributable to the electrochemical reduction of hypophosphite to elemental phosphorous, in spite of the poor physical meaning of this interpretation.

The voltammetric curves obtained with a 0.05 M (4.4 g dm^{-3}) hypophosphite solution exhibited visible plateaus enabling the diffusivity and the kinetic parameters to be estimated (Figure 2). Increasing the concentration of hypophosphite species up to 0.30 M (26.4 g dm^{-3}) showed that the current density varied

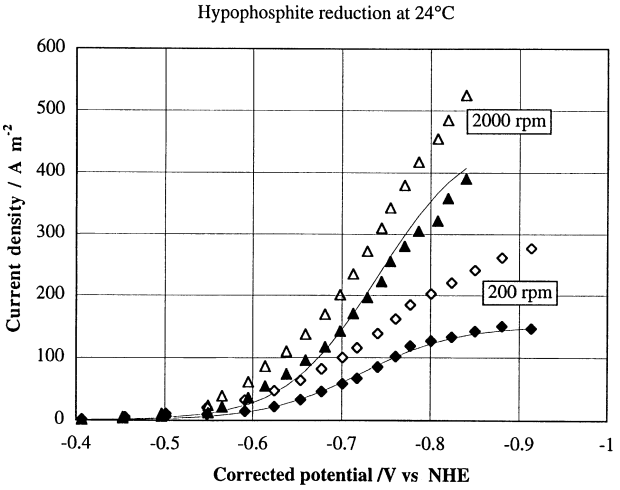

Fig. 2. Voltammetric curves of hypophosphite reduction from a 0.05 M solution. Supporting electrolyte: 0.5 M acetic acid and 0.10 M sodium acetate. Overall current (light symbols) and reduction current (dark symbols) after subtracting the residual current; solid line corresponds to the reduction current fitted with the parameter values given in Table 3.

with $H_2PO_2^-$ concentration only to a low extent and the electrode seemed to be partially blocked at high concentration of the phosphorous containing species. This may partly be the cause of the low dependence of the P-containing agent concentration in the bath on the phosphorous content in the solid over 10–20 g dm^{-3} [4]. The parameters of the reduction were only determined for the lowest hypophosphite concentration (Table 3), assuming one electron is involved in the reduction.

As for nickel deposition, the diffusion coefficients of $H_2PO_2^-$ ion were compared with the corresponding diffusivities at infinite dilution ($\lambda_{H_2PO_2^-} = 46 \times 10^{-4}$ m^2 S mol^{-1} at 25 °C). The expectable deviations between experimental values and D_0 were due to the appreciable ionic strength of the baths. The charge transfer coefficient of the reduction was found to increase with temperature, as for nickel deposition; coefficient α determined at 56 °C was fairly consistent with the value used by Kim and Sohn [22] in their modelling of electroless Ni–P formation at 90 °C (0.80).

3.3. *Ni–P alloy deposition*

Voltammetric curves recorded from a solution containing both electroactive species at 0.05 M were

Table 3. Diffusion coefficient of hypophosphite species and kinetics parameters of hypophosphite reduction from a 0.05 M sodium hypophosphite, 0.10 M sodium acetate and 0.5 M acetic acid containing bath

Temperature /°C	$i_{standard}$ /A m^{-2}	αv_e	$10^9 \times D$ /m^2 s^{-1}	$10^9 \times D_0$ /m^2 s^{-1}
24	2.3×10^{-2}	0.47	0.937	1.19
39	1.2×10^{-2}	0.57	1.26	1.72
56	2.7×10^{-3}	0.85	2.17	2.43

compared with the theoretical current density calculated by summing up the residual contribution and the partial current densities, using Equations 1 and 2 with the parameter values reported in Tables 2 and 3. This method assumed implicitly that each reduction is independent of the other one. Comparison between theory and practice is established on an example in Fig. 3. Because of the comparable values for the rest potentials and the kinetic parameters, the predicted voltammetric curve exhibited only one wave; however an ill-defined plateau was recorded for potentials near −0.65 V vs NHE and one of the two reduction waves appeared to be shifted towards less cathodic potential during the codeposition: the first wave likely corresponded to hypophosphite reduction which is known to be favoured in comparison with nickel deposition at low or moderate current densities.

Besides, the kinetically limited current densities of the individual reduction were plotted versus the electrode potential for various temperature (Fig. 4). Hypophosphite reduction appeared to be favoured at ambient temperature; increasing the solution temperature reduced the deviation between the partial current densities and similar values were predicted at the highest temperature (56 °C). Phosphorous content in the alloy produced may therefore be expected to be affected by temperature.

4. Alloy deposition

Ni–P alloys were prepared varying the operating conditions namely, the electrode potential, the flow velocity in the range 0.06–0.12 m s^{-1}, the amount of hypophosphite, the solution temperature and the irradiation conditions. The deposition time was varied from 10 min to one hour. In a general manner, the range of fluid velocity corresponded to nonestablished laminar flow near the electrode surface and was observed to have a low impact on the deposition. Experimental results were first presented in terms of faradaic yield; the weight content of phosphorous in the alloys produced was then discussed in relation to their aspects and their structures.

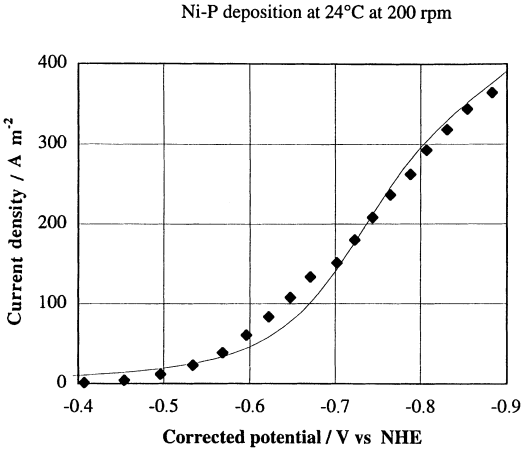

Fig. 3. Voltammetric curves of Ni–P deposition from a 0.05 M Ni acetate, 0.05 M Na hypophosphite solution: comparison of model predictions (solid line) with experimental variations (◆). Supporting electrolyte: 0.5 M acetic acid and 0.10 M sodium acetate.

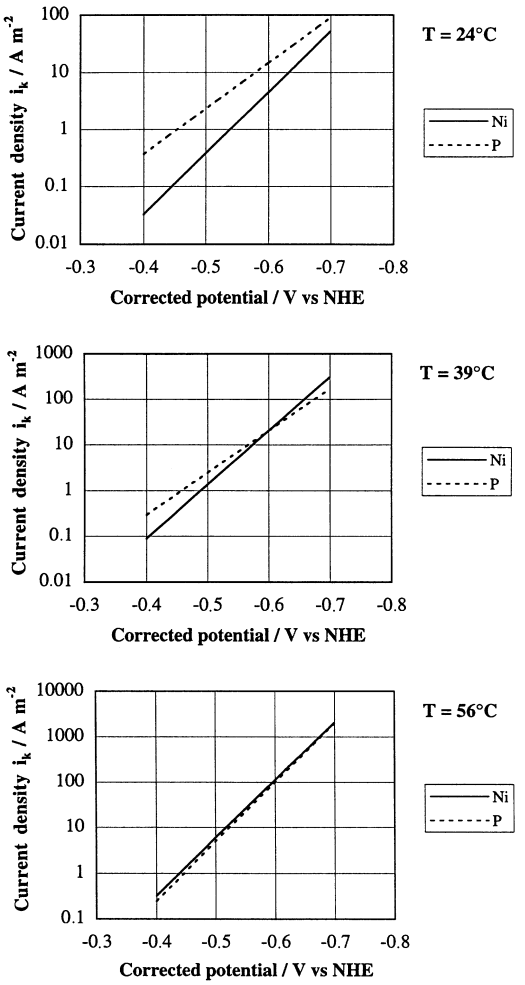

Fig. 4. Theoretical variations of the kinetically limited current densities with potentials for nickel and phosphorous deposition, depending on temperature.

4.1. *Faradaic yield*

Faradaic yield of the alloy deposition was estimated from the nickel weight in the deposit, m_{Ni}, as follows. The faradaic yield for Ni deposition was first calculated from m_{Ni} using the relation:

$$\Phi_{e,Ni} = \frac{m_{Ni} v_{e,Ni} F}{M_{Ni} Q} \quad (4)$$

where M_{Ni} is the molecular weight of nickel and Q the electrical charge passed. The faradaic yield for alloy deposition, Φ_e, was deduced from $\Phi_{e,Ni}$, taking into account the phosphorous weight content, x_p, and the numbers of electrons involved in the two reductions:

$$\Phi_e = \frac{\Phi_{e,Ni}}{\left(1 - x_P \frac{M_P v_{e,P}}{M_{Ni} v_{e,Ni}}\right)} \quad (5)$$

Faradaic yield was correlated to operating current density, in comparison with the limiting current

density. Limiting current densities could not be calculated directly because of the lack of reliable relationship between the reduction current of hypophosphite and its concentration. In addition, only one electron is involved in hypophosphite reduction which reduces the significance of its current density in comparison with that for nickel deposition with the two electron transfer. It was therefore preferred to compare the operating current density with the limiting current density of nickel deposition, $i_{L,Ni}$, neglecting the reduction of hypophosphite ion. The analysis was restricted to the case of the flow cell, with and without laser irradiation.

Mass transfer rates for Ni deposition in the flow cell were estimated from the rates previously measured using the reduction of potassium ferricyanide(III) [10], taking into account the changes in diffusion coefficient, viscosity and electrode length: the presence of hypophosphite was taken into consideration in the value for the viscosity of the codeposition bath (Table 1) whereas the diffusion coefficient was obtained from the voltammetric curves of nickel deposition (Table 2). For the case of a 0.05 M nickel acetate solution with 0.01 M sodium hypophosphite flowing at $0.10\,m\,s^{-1}$, the limiting current $i_{L,Ni}$ was estimated at $90\,A\,m^{-2}$ for experiments conducted without laser beam, and at $125\,A\,m^{-2}$ with laser assistance.

In addition to their estimation from measurements, faradaic yields were predicted regardless of phosphorous deposition. In a first approach, hydrogen evolution was neglected for current densities below the limiting value, $i_{L,Ni}$. Over this limit, the side reaction was assumed to occur independently of nickel deposition and the theoretical faradaic yield was simply calculated as

$$\Phi_e = \frac{i}{i_{L,Ni}} \quad \text{for } i \geqslant i_{L,Ni} \qquad (6)$$

For all cases, laser assistance had a weak influence on the faradaic yield and Fig. 5 shows its variation with the reduced current density $i/i_{L,Ni}$, varying the hypophosphite concentration. For current densities below $i_{L,Ni}$, the current efficiency lay in the range 0.30–0.60, which indicates the significance of hydrogen evolution, in accordance with other work (see [4] and [8] for instance). The values over unity shown in Fig. 5 corresponded to very thin deposits for which the current yield could not be estimated with sufficient accuracy. Despite noticeable scattering due to the different operating conditions, the set of Φ_e values indicated a decreasing tendency with the reduced current density over unity, as expected by Equation 6. In addition, the alloy deposition from concentrated hypophosphite baths was generally carried out with lower current efficiency than from more dilute solutions, whatever the operating current density (Fig. 4): this fact was consistent with the conclusions of previous studies dealing with phosphorous acid whose concentration was varied from a few 10^{-3} M to 0.4 M [1, 4, 8].

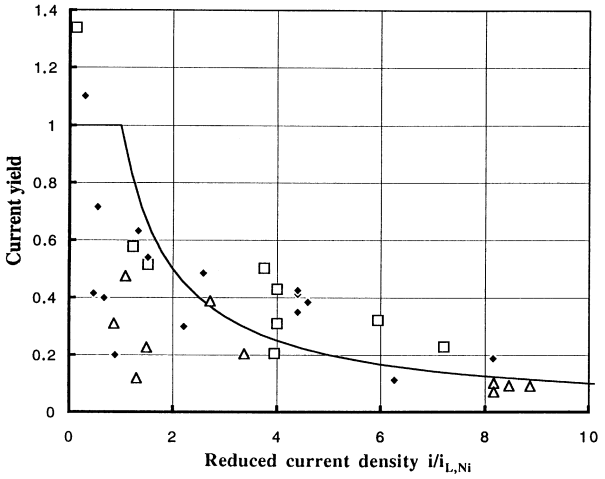

Fig. 5. Theoretical and experimental variations of the current yield for alloy deposition with the reduced current density $i/i_{L,Ni}$, depending on $H_2PO_2^-$ concentration in the electrolytic solution. Experiments carried out with or without laser assistance, at 25 or 50 °C. Key: (□) 0.005 M, (◆) 0.01 M, (△) 0.20 M and (——) theory.

4.2. *Alloys prepared without laser assistance*

The weight phosphorous content in the alloys prepared without laser assistance at 25 °C was plotted against the applied current density in Fig. 6 for the three hypophosphite concentrations. In accordance with previous works, substantial amounts of phosphorous could be codeposited even from dilute solutions of hypophosphite. According to most investigations dealing with $H_2PO_3^-$ reduction [4, 19, 23, 24], x_p is reduced by increasing the current density. The phosphorous content in the alloys produced from hypophosphite solutions did not follow the above conclusions (Fig. 6) as commented below.

Use of the most dilute solution resulted in phosphorous contents varying from 5 to 7.5 wt % without a clear dependence of the applied c.d. The structure of the alloy was quite consistent with Bredael's observations: X-ray diffraction spectra exhibited peaks attributed to pure fcc nickel; the presence of phos-

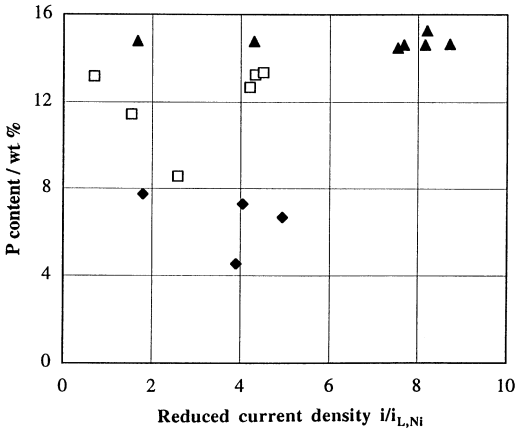

Fig. 6. Phosphorous weight content in the alloys produced without laser assistance at 25 °C depending on the reduced current density and the $H_2PO_2^-$ concentration in the electrolytic bath. Key: (◆) 0.005 M, (□) 0.01 M and (▲) 0.20 M.

phorous in the lattice favoured (1 1 1) reflections and was detrimental to (2 0 0) and (2 2 2) reflections. In addition, deformation of the lattice due to insertion of phosphorous resulted in broader diffraction peaks than for pure nickel deposit, in agreement with previous investigations [19, 23, 24]. The peak of the (1 1 1) reflections was at 52–52.3 ° and its half-width was near 0.8 °. SEM observations revealed the fairly homogeneous aspect of the deposit consisting of circular grains whose diameter varied from 1 μm for current densities below $i_{L,Ni}$ up to 5 μm at 400 A m^{-2}; traces of gas bubbles could be seen at the surface of deposits produced at high current densities. Figure 7 shows the regular morphology of a deposit prepared at $i/i_{L,Ni} = 2.5$.

The alloys prepared with the most concentrated solution (0.20 M) had a phosphorous content near 14.5 wt % in a very large range of current density. The deposits produced were less adherent on the copper substrate. As shown in Fig. 8, the deposits consisted in small grains and presented significant crackings, due to their high phosphorous content and the resulting internal stresses. Amorphous structure was revealed by the very large peaks of (1 1 1) reflections at 52° with a half-width around 7°; in addition, (2 0 0) reflections were totally surpressed, as expected. For a hypophosphite concentration of 0.01 M, the phosphorous content was shown to exhibit a well-marked minimum for reduced current densities near 2.5: current densities either below $i_{L,Ni}$ or far above $i_{L,Ni}$ resulted in phosphorous contents near 13 wt %. The alloys prepared under extreme current densities (c.d.'s) were quite similar – with respect to their aspect and their structure – to the alloys produced from the 0.20 M hypophosphite solution; the density of crackings was, however, reduced. By contrast, deposits obtained at intermediate c.d.'s and with a lower phosphorous content exhibited a more regular aspect with well-defined grains and only a few crackings, in spite of the traces of hydrogen bubbles (Fig. 9); broadening of (1 1 1) peak was hardly visible, indicating that crystalline structure prevailed in the deposit.

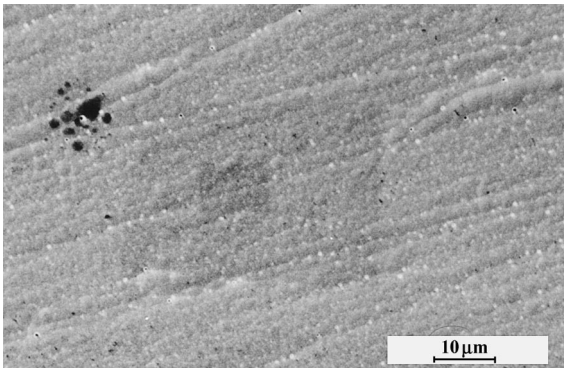

Fig. 7. SEM view of Ni–P produced from a 0.005 M $H_2PO_2^-$ containing bath without laser illumination; $i/i_{L,Ni} = 2.5$; deposit thickness = 5.2 μm.

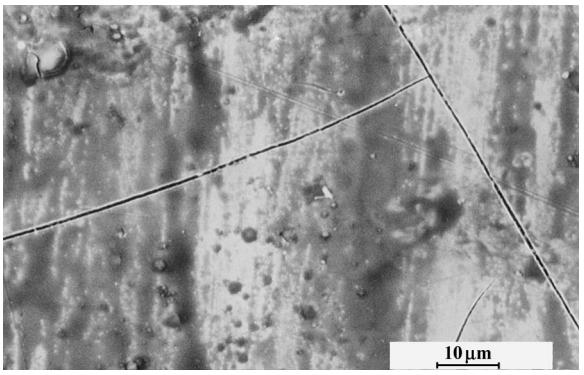

Fig. 8. SEM view of Ni–P produced from a 0.20 M $H_2PO_2^-$ containing bath without laser illumination; $i/i_{L,Ni} = 8.2$; deposit thickness = 3.6 μm.

Heating the electrolytic bath to 50 °C resulted in a 0.6–2% reduction in the phosphorous content; no evident correlation of this reduction with the operating conditions was found. The effect of temperature on the alloy composition was quite consistent with the conclusions drawn from the above electrochemical investigation, regardless of the diffusion control of the two separate depositions. The aspect and the structure of the deposits produced at 50 °C did not differ significantly from those at 25 °C due to the moderate change in phosphorous content observed.

4.3. *Use of a pulsed laser beam*

It was first observed that assistance of a pulsed laser beam largely improved the adherence of the alloys and, for some cases, the deposit could be detached from the substrate surface only by mechanical scraping with emery paper: the periodic rise in temperature might allow diffusion of the matter deposited into the substrate, as observed for zinc [10], in spite of the very different properties of the two systems considered.

Laser assistance was of a weak effect on the alloy composition for low current densities ($i \leqslant 0.5\ i_{L,Ni}$): neither their composition nor their aspect were

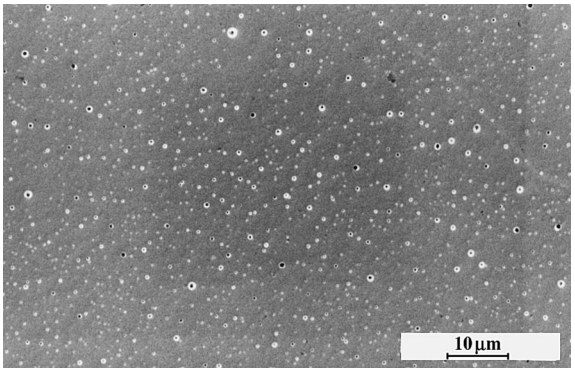

Fig. 9. SEM view of Ni–P produced from a 0.01 M $H_2PO_2^-$ containing bath without laser illumination; $i/i_{L,Ni} = 1.5$; deposit thickness = 8.7 μm.

Table 4. Electrodeposition of Ni–P alloys from a solution containing 0.05 M nickel acetate, 0.10 M sodium acetate and 0.5 M acetic acid: effect of the average power of the pulsed laser beam (spot diameter near 4 mm) on the phosphorous content (in wt %) (Operating current densities, in A m^{-2}, were given in parenthesis)

$[H_2PO_2^-]$ /mol dm^{-3}	*Power, P/W*		
	0	*1*	*2*
0.005	4.5 (316), 7.3 (328)	3.9 (772)	3.5 (812)
0.01	13.3 (356), 13.4 (360)	6.8 (976), 7.1 (976)	6.1 (875)
0.20	14.7 (615), 15.3 (680)	15.1 (1512), 14.7 (1512)	13.4 (1551)

modified to a noticeable extent by the incident pulsed beam. By contrast, the phosphorous content was significantly changed for large current densities, as shown in Table 4. Use of EPMA technique revealed that the deposit composition was not uniform at the surface: the contents given in Table 4 were the averages of 6–10 local measurements at the surface. In particular, for the deposits produced from a 0.20 M hypophosphite solution, the phosphorous content could attain 16 wt % in clusters a few micrometres large. The reduction in the average content due to pulse laser irradiation was of the order of 1 wt % for alloys produced with either low or high concentrations of hypophosphite: the moderate variation of the phosphorous content did not permit change in their structure for both series of deposits. Laser assistance for the 0.01 M $H_2PO_2^-$ solution resulted in large decreases in phosphorous content: the fairly amorphous structure of the alloys produced without laser assistance was replaced by a mainly crystalline structure, revealed by the narrow peaks corresponding to (1 1 1) and (2 0 0) reflections, the latter to a lower extent. The respective peak widths of the double-angle spectra were near 0.8° and 1.2°, respectively.

Deposits produced from solutions with hypophosphite concentrations of 0.005 and 0.01 M exhibited similar aspects, due to comparable current densities (Table 4). The central zone, submitted to a higher flux, had a more regular morphology than the peripheral region where formation of small bubbles could be observed at regular intervals on the surface. In the central zone, deposits consisted in circular large grains, 5–10 μm in diameter, whose limits were less visible than for deposits produced in the dark (Fig. 10): this may be attributed to coalescence phenomena, as observed for zinc deposition [10]. For the most concentrated solution, the high current densities were the cause of intensive hydrogen evolution, which rendered the deposit morphology most irregular. Again, significant coalescence phenomena were observed in the central region with a nearly melted aspect of the grain boundaries whereas the outer surface exhibited a cracked aspect.

4.4. *Use of a continuous laser*

The diameter of the laser beam was half of the electrode size, hence only the central part of the electrode was submitted to the continuous light with an average flux of 1.7×10^4 W m^{-2}. Figure 11 shows typical profiles of phosphorous content. As for the pulsed laser source, stronger effects were observed for high current densities (Fig. 12). The central region of the deposit had a phosphorous content noticeably lower than the peripheral area which was little or not illuminated.

The morphology of the deposits prepared with the argon laser did not differ significantly from those produced in the dark: the grain size was also enhanced by increasing the current density. The limits between two neighbouring grains was nevertheless less visible with laser illumination and coalescence phenomena might also be invoked, however to a lower extent than with the pulsed laser source.

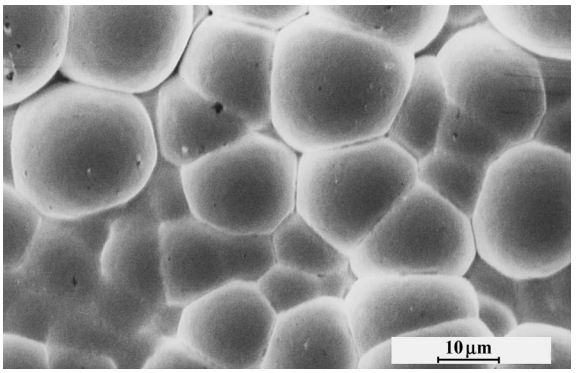

Fig. 10. SEM view of Ni–P produced from a 0.01 M $H_2PO_2^-$ containing bath with assistance of a pulsed laser beam (1 W); $i/i_{L,Ni} = 8.2$; deposit thickness = 12 μm.

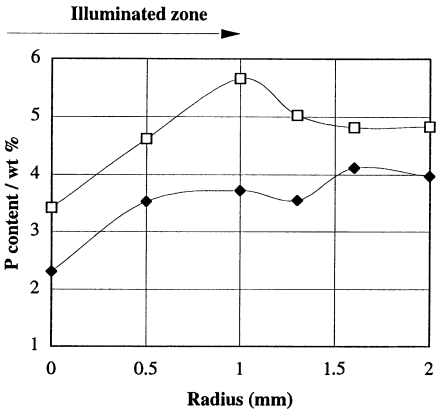

Fig. 11. Experimental profiles of phosphorous weight content in the alloys produced with assistance of argon laser (1.7×10^4 W m^{-2}): only the central zone (radius 1 mm) was submitted to the incident beam. Current density, *i*: (◆) 385 and (□) 685 mA m^{-2}.

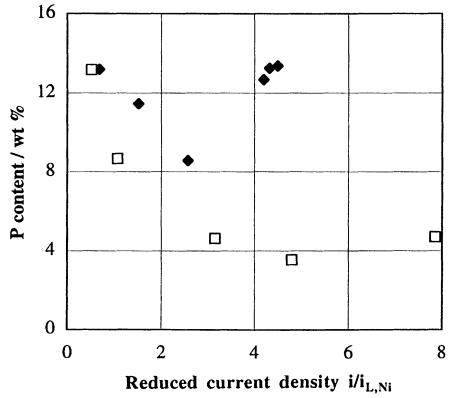

Fig. 12. Phosphorous weight content in the alloys produced at 25 °C depending on the reduced current density: effect of the argon laser beam (1.7×10^4 W m^{-2}). Key: (◆) no laser and (□) argon laser.

5. Conclusions

In agreement with the results of an electrochemical investigation of Ni–P deposition, the temperature rise allowed by an incident laser beam was shown to result in appreciable decrease in the phosphorous content in the alloys deposited. In particular, for the case of a 0.05 M nickel acetate medium with 0.01 M sodium hypophosphite, the amorphous alloy produced under high current densities and without illumination was replaced by a more crystalline material by laser assistance whereas the phosphorous content was reduced from 13 to 7 wt %. The periodic change in temperature of the electrode surface allowed by the pulsed source could not favour the growth of an amorphous phase. The incident laser beam likely decreases the internal stresses in the deposit by reducing the phosphorous content and heating of the depositing surface. In particular, coalescence phenomena, previously put into evidence for the case of zinc deposition under diffusional control, were also observed for high current densities. The effect of a laser beam on the mechanical properties of Ni–P alloys should be confirmed by further investigations.

Acknowledgements

This investigation was sponsored by CNRS through a collaborative programme between Tunisia and France (PICS Nr. 312). The authors are also indebted to J. P. Haeussler (Ecole des Mines, Nancy) for his careful EPMA measurements.

References

[1] E. Bredael, B. Blanpain, J. P. Celis and J. R. Roos, *J. Electrochem. Soc.* **141** (1994) 294.
[2] E. Vafaei-Makhsoos, E. L. Thomas and L. E. Toth, *Metall. Trans. A* **9a** (1978) 1449.
[3] M. Yamamoto, K. Shirai and N. Watanabe, *J. Electrochem. Soc.* **138** (1991) 2082.
[4] A. Brenner, D. E. Couch and E. Kellogs Williams, *J. Res. National Bureau of Standards* **44** (1950) 109.
[5] J.-P. Bonino, P. Pouderoux, C. Rossignol and A. Rousset, *Plat. Surf. Finish.* Apr. (1992) 62.
[6] G. Mc Mahon and U. Erb, *J. Mater. Sci. Lett.* **8** (1989) 865.
[7] K.-W. Lin and J.-K. Ho, *J. Electrochem. Soc.* **139** (1992) 1305.
[8] J.-L. Delplancke, R. Winand, M. Dierickx and L. Lifschitz, *ibid.* **140** (1993) 2800.
[9] J. C. Puippe, R. E. Acosta and R. J. von Gutfeld, *ibid.* **128** (1981) 2539.
[10] I. Zouari, F. Lapicque, M. Calvo and M. Cabrera, *ibid.* **139** (1992) 2163.
[11] J. Newman, *J. Electrochem. Soc.* **113** (1966) 501.
[12] J. Matulis and R. Slizis, *Electrochim. Acta*, **9** (1964) 1177.
[13] I. Epelboin and R. Wiart, *J. Electrochem. Soc.* **118** (1971) 1577.
[14] J. O'M. Bockris, D. Drazic and A. R. Despic, *Electrochim. Acta* **4** (1961) 325.
[15] P. Andricacos, C. Arana, J. Tabib, J. Dukovic and L. T. Romankiw, *J. Electrochem. Soc.* **136** (1989) 1336.
[16] R. C. V. Arvia, A. J. Arvia and J. J. Podesta, *Electrochim. Acta* **14** (1969) 541.
[17] A. Saraby-Reintjes and M. Fleischmann, *ibid.* **29** (1984) 557.
[18] S. Hessami and C. W. Tobias, *J. Electrochem. Soc.* **136** (1989) 3611.
[19] M. Ratzker, D. S. Lahmore and K. W. Pratt, *Plat. Surf. Finish.* (Sept. 1986) 74.
[20] T. M. Harris and Q. D. Dang, *J. Electrochem. Soc.* **140** (1993) 81.
[21] R. L. Zeller III and U. Landau, *ibid.* **139** (1992) 3464.
[22] Y. S. Kim and H.-J. Sohn, *ibid.* **143** (1996) 505.
[23] D. S. Lashmore and J. F. Weinroth, *Plat. Surf. Finish.* (Aug. 1982) 72.
[24] E. Bredael, J. P. Celis and J. R. Roos, *Surf. Coat. Technol.* **58** (1993) 63.